

# The Impact of Interlayer Electronic Coupling on Charge Transport in Organic Semiconductors: A Case Study on Titanylphthalocyanine Single Crystals

Zongpeng Zhang, Lang Jiang, Changli Cheng, Yonggang Zhen,\* Guangyao Zhao, Hua Geng, Yuanping Yi,\* Liqiang Li, Huanli Dong, Zhigang Shuai, and Wenping Hu\*

Dedicated to the Institute of Chemistry, Chinese Academy of Sciences, on the occasion of its 60th anniversary

**Abstract:** Traditionally, it is believed that three-dimensional transport networks are preferable to those of lower dimensions. We demonstrate that inter-layer electronic couplings may result in a drastic decrease of charge mobilities by utilizing field-effect transistors (FET) based on two phases of titanyl phthalocyanine (TiOPc) crystals. The  $\alpha$ -phase crystals with electronic couplings along two dimensions show a maximum mobility up to  $26.8 \text{ cm}^2 \text{ V}^{-1} \text{ s}^{-1}$ . In sharp contrast, the  $\beta$ -phase crystals with extra significant inter-layer electronic couplings show a maximum mobility of only  $0.1 \text{ cm}^2 \text{ V}^{-1} \text{ s}^{-1}$ . Theoretical calculations on the bulk crystals and model slabs reveal that the inter-layer electronic couplings for the  $\beta$ -phase devices will diminish remarkably the device charge transport abilities owing to the coupling direction perpendicular to the current direction. This work provides new insights into the impact of the dimensionality and directionality of the packing arrangements on charge transport in organic semiconductors.

Charge transport in organic semiconductors is one of key issues in organic optoelectronics since the discovery of conducting polymers in 1970s.<sup>[1]</sup> Molecular packing arrangements not only can have an important influence on reorgan-

ization energy and electronic coupling (absolute transfer integral),<sup>[2]</sup> but also provide different transport networks.<sup>[3]</sup> Tremendous efforts including chemical structure tailoring and crystal polymorphic controlling have been devoted to tuning molecular packing.<sup>[4]</sup> In contrast to one-dimensional (1D) and 2D common packing arrangements (Supporting Information, Figure S1), molecular packing that constitutes a 3D molecular framework has been rarely explored in construction of organic FETs.<sup>[5]</sup> It should be noteworthy that the directionality and dimensionality of electronic couplings in the packing arrangements is of great importance to charge transport behaviors. Traditionally, it is believed that 3D transport networks would be superior to lower-dimensional networks.<sup>[6]</sup>

As a well-known organic semiconductor and photoconductor, titanyl phthalocyanine (TiOPc) is a nonplanar polar  $\pi$ -conjugated molecule with pyramid configuration (Figure 1a, inset). Very interestingly, the TiOPc molecules can crystallize in either a 2D lamellar brickstone motif for the  $\alpha$  phase or an unusual 3D framework for the  $\beta$  phase.<sup>[7]</sup> Herein, we demonstrate that the sheet-shaped  $\alpha$  phase single crystals

[\*] Z. P. Zhang, Prof. Y. G. Zhen, Dr. G. Y. Zhao, Prof. H. Geng, Prof. Y. P. Yi, Prof. H. L. Dong, Prof. W. P. Hu  
Institute of Chemistry, Chinese Academy of Sciences (ICCAS)  
Beijing 100190 (China)  
E-mail: zhenyg@iccas.ac.cn  
ypyi@iccas.ac.cn  
huwp@iccas.ac.cn

Dr. L. Jiang  
Cavendish Laboratory, University of Cambridge  
JJ Thomson Avenue, Cambridge CB3 0HE (UK)  
Prof. L. Q. Li  
Advanced Nanomaterials Division, Suzhou Institute of Nano-tech and Nano-bionics, CAS  
Suzhou, 215123 (China)  
C.L. Cheng, Prof. Z. G. Shuai  
Department of Chemistry, Tsinghua University  
Beijing 100080 (China)  
Prof. W. P. Hu  
Key laboratory of Molecular Optoelectronic Sciences, School of Science, Tianjin University & Collaborative Innovation Center of Chemical Science and Engineering  
Tianjin 300072 (China)

Supporting information for this article can be found under:  
<http://dx.doi.org/10.1002/anie.201601065>.

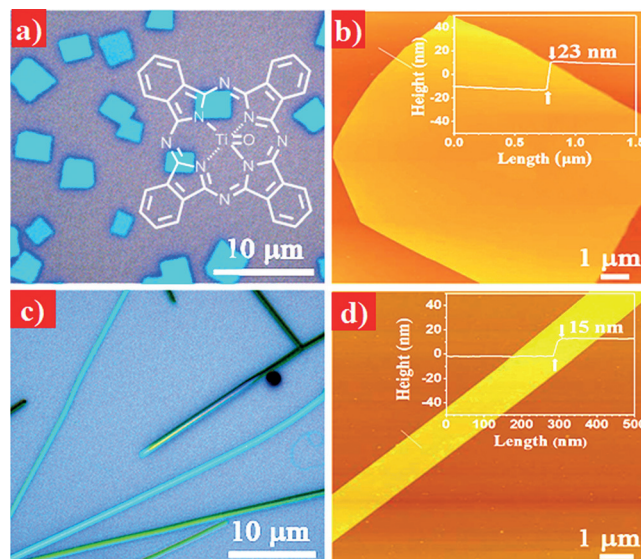


**Figure 1.** Crystal morphologies of two phases of TiOPc. a), b) Optical and AFM images of  $\alpha$ -TiOPc sheet crystals (thickness 20–35 nm). Inset of (a): molecular structure of TiOPc with a pyramid configuration. c), d) Optical and AFM images of  $\beta$ -TiOPc ribbon crystals (thickness 15–35 nm).

with distinct transfer integrals in the 2D semiconducting channel show a remarkable hole mobility of up to  $26.8 \text{ cm}^2 \text{ V}^{-1} \text{ s}^{-1}$ , which is among the highest values for p-type organic semiconductors with excellent air stability. On the other hand, the microribbon-shaped  $\beta$ -phase single crystals present drastically diminished mobilities as low as  $0.1 \text{ cm}^2 \text{ V}^{-1} \text{ s}^{-1}$  along the crystal growth direction owing to destructive inter-layer interferences that arise from the significant electronic couplings perpendicular to the current direction.

The TiOPc crystals are prepared by physical vapor transport (PVT) technique through a two-zone horizontal tube furnace (Supporting Information, Figure S2).<sup>[8]</sup> Sheet crystals are obtained on the substrate at the temperature zone of about  $210^\circ\text{C}$ , while ribbon crystals are grown at the temperature zone at about  $180^\circ\text{C}$ . The sheet crystals are mostly rectangular in shape (Figure 1 a) with a size of 2–20  $\mu\text{m}$  and thickness of 20–35 nm (Figure 1 b), as identified by atomic force microscopy (AFM) measurements. The crystal surface is very flat with a root-mean-square (RMS) roughness of 0.2–0.4 nm, indeed flat at the atomic level. The ribbon crystals are 0.5–2  $\mu\text{m}$  in width, 20–120  $\mu\text{m}$  in length (Figure 1 c), and 15–35 nm in thickness (Figure 1 d).

To further confirm the molecular packing in microsheet and nanoribbon crystals, powder X-ray diffraction (XRD), selected-area electron diffraction (SAED), and Raman spectroscopy were performed, respectively. XRD results are shown in Figure 2 a. For microsheets, the intense peak at  $7.48^\circ$  ( $d = 11.80 \text{ \AA}$ ) and the higher-order reflections at  $15.12^\circ$  ( $d = 5.86 \text{ \AA}$ ) and  $22.82^\circ$  ( $d = 3.90 \text{ \AA}$ ) are assigned to the diffractions of (010), (020), and (030) lattice planes of  $\alpha$ -TiOPc, respectively.<sup>[7,9]</sup> As for nanoribbons, a sharp reflection at  $6.88^\circ$  ( $d = 12.83 \text{ \AA}$ ) is attributed to the diffractions of (100) lattice planes of  $\beta$ -TiOPc, indicating the nanoribbons are  $\beta$ -

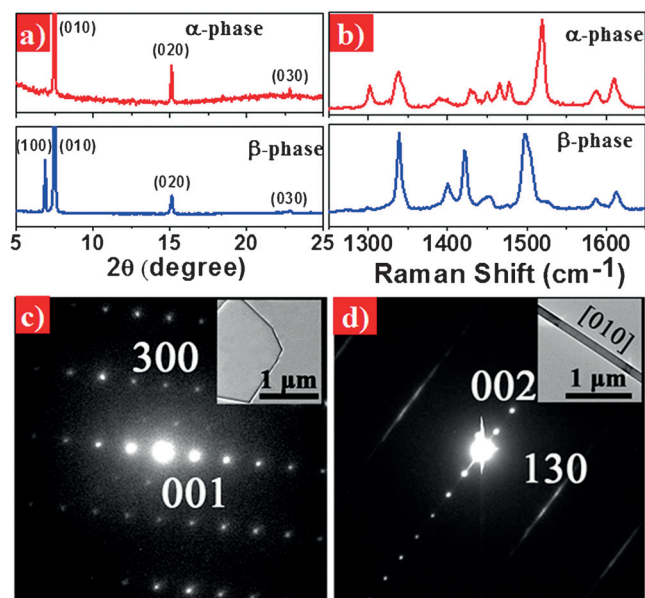


**Figure 2.** a) X-ray powder diffraction patterns and b) Raman spectra of sheet and ribbon crystals, which are identified as  $\alpha$ -TiOPc and  $\beta$ -TiOPc crystals, respectively. c), d) TEM images and SAED patterns of microsheet (c,  $\alpha$ -TiOPc) and nanoribbon (d,  $\beta$ -TiOPc) crystals.

phase TiOPc.<sup>[9]</sup> Furthermore, the crystals are subtly different in Raman spectra at the sensitive region around  $1500 \text{ cm}^{-1}$  derived from the pyrrole stretching modes, which is very sensitive to the crystalline structure.<sup>[10]</sup> As shown in Figure 2 b, the  $\alpha$ -TiOPc sheets have a characteristic peak at  $1519 \text{ cm}^{-1}$ , while the  $\beta$ -TiOPc ribbons exhibit a peak at  $1500 \text{ cm}^{-1}$ . Transmission electronic microscopy (TEM) images and selected-area electron diffraction (SAED) patterns of microsheets and nanoribbons are shown in Figure 2 c and d, respectively, which are indexed to the lattice constants of  $\alpha$ -phase and  $\beta$ -phase. The ideal  $\pi$ - $\pi$  direction for microsheet crystals is along  $[10\bar{1}]$ , whereas the nanoribbon crystals are grown along the  $[010]$  direction.

Charge-transport properties of  $\alpha$ -microsheets along the  $[10\bar{1}]$  direction and  $\beta$ -nanoribbons along the  $[010]$  direction are examined by field-effect transistors by utilizing the “organic ribbon mask” technique (Figure 3 a,b; Supporting Information, Figure S3).<sup>[11]</sup> It can be deduced from Figure 2 that TiOPc molecules adopt an “edge-on” style with an orientation angle of  $62^\circ$  and  $80^\circ$  to the substrate for  $\alpha$ -TiOPc and  $\beta$ -TiOPc crystals, respectively.<sup>[9,12]</sup> All devices are measured in air at room temperature. Typical transfer and output characteristics of the devices are shown in Figure 3 c,d. As for

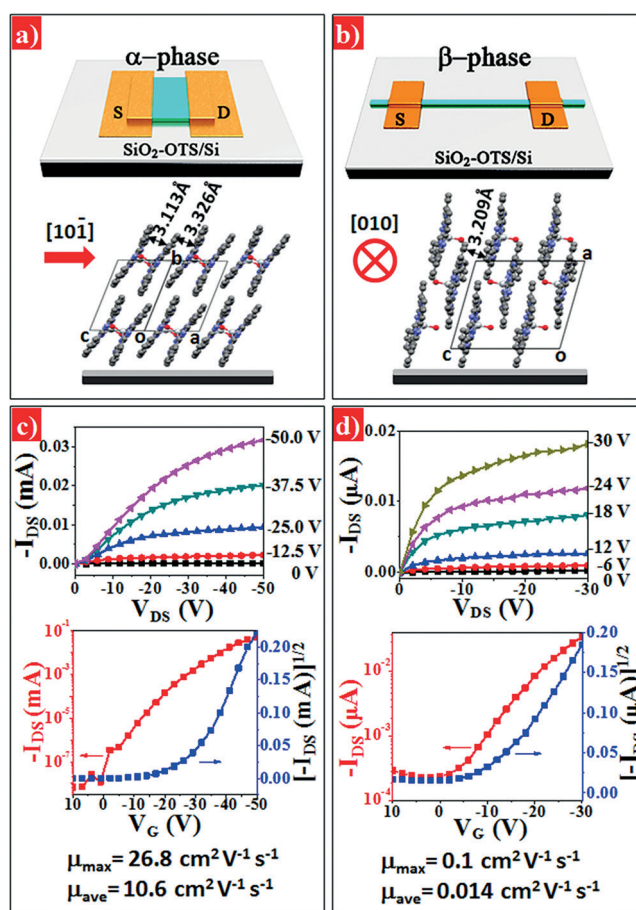


**Figure 3.** a), b) Diagrams of device configurations based on  $\alpha$ -TiOPc (a) and  $\beta$ -TiOPc (b) and molecular arrangements of  $\alpha$ - and  $\beta$ -TiOPc on the OTS modified SiO<sub>2</sub>/Si substrate. c), d) Typical output and transfer characteristics of OFETs based on  $\alpha$ -TiOPc ( $V_{DS} = -50 \text{ V}$ ) (c) and  $\beta$ -TiOPc ( $V_{DS} = -30 \text{ V}$ ) (d).

$\alpha$ -microsheets (Figure 3c; Supporting Information, Figure S4), the transistor channel length is 1.6–8  $\mu\text{m}$ , and the channel width is in the range of 6–25  $\mu\text{m}$ . The maximum mobility reaches  $26.8 \text{ cm}^2 \text{ V}^{-1} \text{ s}^{-1}$  and the average mobility is  $10.6 \text{ cm}^2 \text{ V}^{-1} \text{ s}^{-1}$  (the mobility distribution of 220 devices for  $\alpha$ -TiOPc is shown in the Supporting Information, Figure S5a) with current on/off ratio at  $10^4$ – $10^7$ . In the case of  $\beta$ -TiOPc (Figure 3d), the channel length is 2–10  $\mu\text{m}$ , and the channel width is from 500 nm to 2  $\mu\text{m}$ . The average mobility is  $1.4 \times 10^{-2} \text{ cm}^2 \text{ V}^{-1} \text{ s}^{-1}$  (the mobility distribution of 15 devices for  $\beta$ -TiOPc is shown in the Supporting Information, Figure S5b) with current on/off ratio at  $10$ – $10^3$ . The devices show the maximum mobility of  $0.1 \text{ cm}^2 \text{ V}^{-1} \text{ s}^{-1}$  with on/off ratio of  $1.2 \times 10^2$ . Obviously, the highest mobility of  $\alpha$ -phase devices is 268 times higher than that of  $\beta$ -phase devices and the average mobility of  $\alpha$ -phase is even 572 times higher than that of  $\beta$ -phase devices.

What causes this huge difference in charge transport between the  $\alpha$  and  $\beta$ -phase TiOPc crystals? From the perspective of molecular arrangements, both phases have an alternate stacking of convex- and concave-type dimers. There are ultra-close  $\pi$ - $\pi$  interactions with short C–C contacts of ca.  $3.2 \pm 0.1 \text{ \AA}$  for both convex and concave pairs in two phases, which is obviously shorter compared to most organic semiconductors.<sup>[4c,13–17]</sup> The molecular concave overlap is similar in two phases, whereas the molecules overlap at both sides in the convex pair of  $\alpha$ -TiOPc but only at the periphery in the case of  $\beta$ -TiOPc (Supporting Information, Figures S6). In the  $\alpha$ -phase crystal, TiOPc molecules form a layer-by-layer lamellar structure, where each molecular plane is almost perpendicular to the current  $[10\bar{1}]$  direction and each layer is parallel to the device substrate surface ( $ac$  plane; Figure 3a). Within one layer each molecule contacts with four neighbors to form two concave and two convex molecular pairs. The center-to-center intermolecular distances are 8.26 and 7.60  $\text{\AA}$  for the convex pairs and 5.18 and 12.14  $\text{\AA}$  for the concave pairs, and the corresponding electronic couplings for hole transport are 42 and 130 meV and 59 and 6 meV, respectively (Figure 4a,c). As expected, the valence band dispersion is strong along the  $\Gamma$ -X and  $\Gamma$ -Z directions but relatively flat along the  $\Gamma$ -Y direction (Supporting Information, Figure S7a). Consequently, the hole effective mass in the  $[10\bar{1}]$  ( $a$ - $c$ ) direction ( $m_{a-c}$ ) is estimated to be  $1.23 m_0$  (Supporting Information, Table S1).

For the  $\beta$ -phase crystal, each TiOPc molecule has six neighbors to form two concave and four convex pairs. The two concave dimers exhibit intermolecular distances of 8.90 and 6.23  $\text{\AA}$  and hole couplings of 37 and 87 meV, respectively. In the case of convex pairs, the intermolecular distances and hole couplings are 9.90  $\text{\AA}$  and 29 meV and 10.08  $\text{\AA}$  and 6 meV for each of two equivalent pairs. (Figure 4b,d) The four convex connections spread in the  $ab$  plane, constituting a layer with the equivalent and inequivalent connections propagating along the  $b$  and  $a$  direction, respectively. We note that the molecular layer is vertical to the device substrate surface ( $bc$  plane) and the TiOPc molecular plane appears to be parallel to the current  $[010]$  direction (Figure 3b). Interestingly, the 2D buckling convex-pair layer are linked by the two different concave pairs alternately stacking along the  $a$  direction, leading to a 3D molecular framework. As a result, the

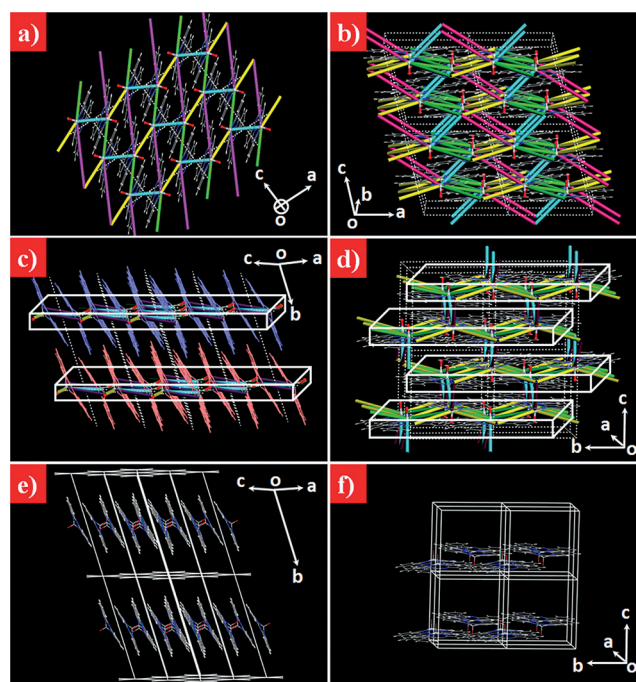


**Figure 4.** Illustration of electronic coupling networks for a), c)  $\alpha$ -microsheet (bold lines: green 42, yellow 130, cyan 59, pink 6 meV) and b), d)  $\beta$ -nanoribbon crystals (b, d: green 6, yellow 29, cyan 87, pink 37 meV). e), f) Models for the  $\alpha$ -TiOPc slab (e: the lattice parameter along the  $b$  axis is elongated as twice that of the unit cell) and  $\beta$ -TiOPc slab (f: half number of molecules are removed from the unit cell); white void cuboids in (c) and (d) represent the respective layers for  $\alpha$  and  $\beta$ -TiOPc.

dispersions of the valence band are considerable in all the three dimensions, especially along the  $\Gamma$ -X direction (Supporting Information, Figure S7b). Interestingly, in the  $[010]$  ( $b$ ) direction for the  $\beta$ -phase crystal, the effective mass  $m_b$  is estimated to be  $6.63 m_0$ , which is over five times larger than  $m_{a-c}$  for the  $\alpha$ -phase crystal (Supporting Information, Table S1). This is consistent with the much lower hole mobilities measured for the  $\beta$ -phase crystal-based devices.

To further elucidate the influence of the directionality and dimensionality of the packing arrangements, we have carried out calculations on model slabs derived from the  $\alpha$  and  $\beta$  crystals (Figure 4e,f). As expected, the band structures for the  $\alpha$  slab are very similar to the  $\alpha$  phase crystal, and the effective masses including  $m_{a-c}$  can be hardly changed owing to lack of inter-layer electronic couplings in the  $\alpha$ -phase crystal. Because of important contribution to the  $a$ -direction transport from the inter-layer concave couplings, the effective mass in the  $a$ -direction ( $m_a$ ) is substantially decreased for the  $\beta$ -phase crystal ( $1.01 m_0$ ) with respect to the  $\beta$  slab ( $4.18 m_0$ ). On the contrary, it is surprising to find that, the  $m_b$  for the  $\beta$  phase crystal is over three times larger than that for the  $\beta$  slab ( $2.21 m_0$ ) in the presence of the inter-layer concave couplings (Supporting Information, Table S1). This should be due to a perpendicular destructive interference of the inter-layer coupling pathways with charge transport behaviors along the  $b$ -direction.<sup>[18]</sup> To the best of our knowledge, for the first time we demonstrate experimentally that charge transport will be diminished by perpendicular inter-layer couplings.

At this point, we notice that the experimental measurements show more inferior transport performance for the  $\beta$  phase with respect to  $\alpha$  phase devices. On one hand, this might be because the detrimental and fast transport in the  $a$ -direction would facilitate charge carriers to be trapped by defects at the semiconductor surface or interface. On the other hand, thermal fluctuation and oxygen doping at ambient conditions could have a profound influence on charge transport.<sup>[2b,19]</sup>

In summary, we have investigated charge transport in the single-crystal field-effect transistors based on two phases of TiOPc crystals. In the  $\alpha$ -microsheet crystals, charges transport with the highest mobility up to  $26.8 \text{ cm}^2 \text{ V}^{-1} \text{ s}^{-1}$  and average mobility of  $10.6 \text{ cm}^2 \text{ V}^{-1} \text{ s}^{-1}$ . In sharp contrast, the carrier mobilities for the  $\beta$ -nanoribbon crystals are at least two orders of magnitude lower, showing the highest mobility of only  $0.1 \text{ cm}^2 \text{ V}^{-1} \text{ s}^{-1}$  and average mobility of  $0.014 \text{ cm}^2 \text{ V}^{-1} \text{ s}^{-1}$ . Theoretical calculations demonstrate that the strong interlayer electronic couplings perpendicular to the current direction, will diminish remarkably the charge transport owing to destructive interference effects. This work provides a deeper understanding of the impact of the dimensionality of packing arrangements and underlines the importance of the directionality of electronic couplings, which is important for molecular design and device optimizations for three-dimensional organic semiconductors.

## Acknowledgements

The authors are grateful to Prof. Eiichi Nakamura (University of Tokyo), Prof. Jianpu Wang and Dr. Yuanyuan Hu (University of Cambridge), Prof. Qingxin Tang (Northeast Normal University), and Prof. Tao Li (Shanghai Jiao Tong University) for profound discussions. The authors acknowledge financial support from National Natural Science Foundation of China (91222203, 21473222, 51303185), the Ministry of Science and Technology of China (2013CB933500, 2015CB856502), and the Strategic Priority Research Program (Grant No. XDB12000000) of the Chinese Academy of Sciences.

**Keywords:** charge transport · crystal polymorphs · organic semiconductors · phthalocyanine

**How to cite:** *Angew. Chem. Int. Ed.* **2016**, *55*, 5206–5209  
*Angew. Chem.* **2016**, *128*, 5292–5295

- [1] a) C. K. Chiang, C. R. Fincher, Y. W. Park, A. J. Heeger, H. Shirakawa, E. J. Louis, S. C. Gau, A. G. MacDiarmid, *Phys. Rev. Lett.* **1977**, *39*, 1098; b) Y. Shirota, H. Kageyama, *Chem. Rev.* **2007**, *107*, 953; c) A. R. Murphy, J. M. J. Frechet, *Chem. Rev.* **2007**, *107*, 1066; d) A. P. Kulkarni, C. J. Tonzola, A. Babel, S. A. Jenekhe, *Chem. Mater.* **2004**, *16*, 4556; e) J. M. Nunzi, *C. R. Phys.* **2002**, *3*, 523.
- [2] a) J. L. Bredas, J. P. Calbert, D. A. da Silva, J. Cornil, *Proc. Natl. Acad. Sci. USA* **2002**, *99*, 5804; b) V. Coropceanu, J. Cornil, D. A. da Silva Filho, Y. Olivier, R. Silbey, J.-L. Brédas, *Chem. Rev.* **2007**, *107*, 926; c) S. M. Ryno, C. Risko, J. L. Bredas, *J. Am. Chem. Soc.* **2014**, *136*, 6421.
- [3] a) V. C. Sundar, J. Zaumseil, V. Podzorov, E. Menard, R. L. Willett, T. Someya, M. E. Gershenson, J. A. Rogers, *Science* **2004**, *303*, 1644; b) R. Zeis, C. Besnard, T. Siegrist, C. Schlockermann, X. Chi, C. Kloc, *Chem. Mater.* **2006**, *18*, 244; c) J. Y. Lee, S. Roth, Y. W. Park, *Appl. Phys. Lett.* **2006**, *88*, 252106; d) C. Reese, Z. Bao, *Adv. Mater.* **2007**, *19*, 4535; e) R. Li, L. Jiang, Q. Meng, J. Gao, H. Li, Q. Tang, M. He, W. Hu, Y. Liu, D. Zhu, *Adv. Mater.* **2009**, *21*, 4492; f) L. Wang, G. Nan, X. Yang, Q. Peng, Q. Li, Z. Shuai, *Chem. Soc. Rev.* **2010**, *39*, 423; g) T. He, X. Zhang, J. Jia, Y. Li, X. Tao, *Adv. Mater.* **2012**, *24*, 2171.
- [4] a) M. Mas-Torrent, C. Rovira, *Chem. Rev.* **2011**, *111*, 4833; b) J. E. Anthony, *Org. Lett.* **2002**, *4*, 15; c) C. Wang, H. Dong, W. Hu, Y. Liu, D. Zhu, *Chem. Rev.* **2012**, *112*, 2208; d) H. Dong, X. Fu, J. Liu, Z. Wang, W. Hu, *Adv. Mater.* **2013**, *25*, 6158; e) A. Brillante, I. Bilotti, R. G. Della Valle, E. Venuti, A. Girlando, *CrystEngComm* **2008**, *10*, 937; f) G. Giri, E. Verploegen, S. C. Mannsfeld, S. Atahan-Evrenk, H. Kim do, S. Y. Lee, H. A. Becerril, A. Aspuru-Guzik, M. F. Toney, Z. Bao, *Nature* **2011**, *480*, 504; g) P. He, Z. Tu, G. Zhao, Y. Zhen, H. Geng, Y. Yi, Z. Wang, H. Zhang, C. Xu, J. Liu, X. Lu, X. Fu, Q. Zhao, X. Zhang, D. Ji, L. Jiang, H. Dong, W. Hu, *Adv. Mater.* **2015**, *27*, 825.
- [5] a) T. Vehoff, B. Baumeier, A. Troisi, D. Andrienko, *J. Am. Chem. Soc.* **2010**, *132*, 11702; b) M. J. Kang, T. Yamamoto, S. Shinamura, E. Miyazaki, K. Takimiya, *Chem. Sci.* **2010**, *1*, 179; c) H. Pang, F. Vilela, P. J. Skabara, J. J. W. McDouall, D. J. Crouch, T. D. Anthopoulos, D. D. C. Bradley, D. M. de Leeuw, P. N. Horton, M. B. Hursthouse, *Adv. Mater.* **2007**, *19*, 4438; d) J. Roncali, P. Leriche, A. Cravino, *Adv. Mater.* **2007**, *19*, 2045; e) P. J. Skabara, J.-B. Arlin, Y. H. Geerts, *Adv. Mater.* **2013**, *25*, 1948.
- [6] W. Wu, Y. Liu, D. Zhu, *Chem. Soc. Rev.* **2010**, *39*, 1489.
- [7] a) W. Hiller, J. Strähle, W. Kobel, M. Hanack, *Z. Kristallogr.* **1982**, *159*, 173; b) T. Enokida, R. Hirohashi, T. Nakamura, *J. Imaging Sci.* **1990**, *34*, 234; c) H. Yonehara, C. Pac, *Mater. Res. Soc. Symp. Proc.* **1994**, *328*, 301.
- [8] R. A. Laudise, C. Kloc, P. G. Simpkins, T. Siegrist, *J. Cryst. Growth* **1998**, *187*, 449–454.
- [9] H. Yonehara, H. Etori, M. K. Engel, M. Tsushima, N. Ikeda, T. Ohno, C. Pac, *Chem. Mater.* **2001**, *13*, 1015.
- [10] C. A. Jennings, R. Aroca, G. J. Kovacs, C. Hsiao, *J. Raman Spectrosc.* **1996**, *27*, 867.
- [11] L. Jiang, J. Gao, E. Wang, H. Li, Z. Wang, W. Hu, L. Jiang, *Adv. Mater.* **2008**, *20*, 2735.
- [12] L. Li, Q. Tang, H. Li, X. Yang, W. Hu, Y. Song, Z. Shuai, W. Xu, Y. Liu, D. Zhu, *Adv. Mater.* **2007**, *19*, 2613.
- [13] J. E. Anthony, *Chem. Rev.* **2006**, *106*, 5028.
- [14] S. Ando, J. Nishida, E. Fujiwara, H. Tada, Y. Inoue, S. Tokito, Y. Yamashita, *Chem. Mater.* **2005**, *17*, 1261.
- [15] M. D. Curtis, J. Cao, J. W. Kampf, *J. Am. Chem. Soc.* **2004**, *126*, 4318.
- [16] J. K. Politis, J. C. Nemes, M. D. Curtis, *J. Am. Chem. Soc.* **2001**, *123*, 2537.
- [17] X. C. Li, H. Sirringhaus, F. Garnier, A. B. Holmes, S. C. Moratti, N. Feeder, W. Clegg, S. J. Teat, R. H. Friend, *J. Am. Chem. Soc.* **1998**, *120*, 2206.
- [18] L. Zhu, V. Coropceanu, Y. Yi, B. Chilukuri, T. R. Cundari, J.-L. Brédas, *J. Phys. Chem. Lett.* **2013**, *4*, 2186.
- [19] R. W. I. de Boer, A. F. Stassen, M. F. Craciun, C. L. Mulder, A. Molinari, S. Rogge, A. F. Morpurgo, *Appl. Phys. Lett.* **2005**, *86*, 262109.

Received: January 30, 2016

Published online: March 17, 2016